RSC Advances

PAPER

View Article Online
View Journal | View Issue

Cite this: *RSC Adv.*, 2020, **10**, 17180

$La_2O_2CO_3:Tb^{3+}$ one-dimensional nanorod with green persistent luminescence

Xiaojing Dou,[a] Yang Li, *[a] Ru Kang,[a] Huiwang Lian[a] and Zhenzhang Li[b]

Received 29th February 2020
Accepted 14th April 2020

DOI: 10.1039/d0ra01926g

rsc.li/rsc-advances

Trivalent terbium-doped oxycarbonate ($La_2O_2CO_3$:1%Tb^{3+}) one-dimensional nanorods are synthesized *via* a facile precipitation method. The average length of $La_2O_2CO_3$:1%Tb^{3+} nanorods is 184.5 nm. Doping Tb^{3+} ions led to several visible emission peaks at 486 nm, 542 nm, and 587 nm under excitation of 258 nm wavelength light. The green afterglow at 542 nm can be detected almost 600 s after ceasing the UV-light irradiation. It can be calculated that the $La_2O_2CO_3$:1%Tb^{3+} sample has one shallow trap depth (E = 0.848 eV) by measuring the thermoluminescence. All the results indicate that a simple precipitation method can synthesize a one-dimensional nanorod with green persistent luminescence.

Introduction

Persistent luminescent nanoparticles (PLNPs) are types of optical materials that have plenty of crystal defects as the charge-trappers. PLNPs can store charge carriers (electrons and holes) under excitation with ultraviolet (UV) radiation and then release subsequently for several seconds, minutes and even hours.[1–4] PLNPs are playing an important role in multi-disciplinary fields because of their broad applications, such as in safety signage, night-vision surveillance, latent fingerprint images, decoration and biomedicine.[5–9]

Nowadays, only a few terbium doped bulk-phosphors such as $Lu_2O_3:Tb^{3+}$,[10] $SrAl_2O_4:Tb^{3+}$ *etc*,[11] have demonstrated their green afterglow. The synthesis method of these materials is a solid-state method, yet almost no successful chemical route can be traced to perfect the size, morphology and dispersion for PLNPs.[10–14] However, the effective combination of nanostructure and rare earth doped persistent luminescent materials are the valid ways to expand the development of PLNPs in the multi-disciplinary fields.[15–17] For example, it had been reported many PLNPs with excellent morphology and size properties synthesized *via* effectively chemical methods, which have shown great application potential in the field of biology.[2,18–22] Therefore, it is necessary and meaningful to find a method of synthesizing a green PLNPs with controllability morphology and uniform dispersity. Furthermore, the inorganic compounds: $La_2O_2CO_3$ are used to be host materials. Because rare-earth doping $La_2O_2CO_3$ can be substituted for La^{3+} ions homogeneously and cannot change host crystal structures, as well as bringing good luminescent properties and high chemical stability.[12,23]

In this research, the green $La_2O_2CO_3$:1%Tb^{3+} PLNPs are prepared *via* a facile precipitation method which appear to be uniformly rod-shaped (length: 50–200 nm, uniform and regular). The $La_2O_2CO_3$:1%Tb^{3+} nanorods exhibit a visible emission at 486 nm, 542 nm, and 587 nm under 258 nm excitation. The green afterglow at 542 nm can be detected almost 600 s after ceasing the UV-light irradiation. The thermoluminescence (ThL) spectrum reveals that $La_2O_2CO_3$:1%Tb^{3+} nanorods have a shallow trap depth at 0.848 eV.

Experiment methods

Sample preparation

Chemicals and materials. The initial rare-earth nitrates, including $La(NO)_3\cdot 6H_2O$ (99.99%) and $Tb(NO_3)_3\cdot 6H_2O$ (99.99%) were purchased from Shanghai Aladdin Biochemical Technology Company, and NH_4OH (25 wt%) was purchased from Tianjin Zhiyuan Chemical Reagent Company, and anhydrous ethanol was purchased from Sinopharm Chemical Reagent Company. All chemicals were of analytical-grade reagents and were used directly without further purification.

Preparation of $La_2O_2CO_3$:1%Tb^{3+}. The $La_2O_2CO_3$:1%Tb^{3+} nanorods were compounded by a precipitation method.[23,24] Firstly, 0.01 mol of $La(NO_3)_3\cdot 6H_2O$ and 0.0001 mol of $Tb(NO_3)_3\cdot 6H_2O$ were added to 100 mL of deionized water followed through vigorous stirring for 10 min. Secondly, NH_4OH (25 wt%) was added to the mixture to reach the pH = 10. Finally, the mixture in a beaker, wrapped with a polyethylene film, was heated in a water bath at 90 °C for 2 h and heavily stirred and then cooled to room temperature. The precursor products $La(OH)_3$:1%Tb^{3+} nanorods were obtained by washing the resulting precipitates with deionized water and anhydrous ethanol respectively for three times, and then dried at 80 °C for

[a]*School of Physics and Optoelectronic Engineering, Guangdong University of Technology, Guangzhou 510006, China*

[b]*College of Mathematics and Systems Science, Guangdong Polytechnic Normal University, No. 293, Zhongshan Avenue West, Tianhe District, Guangzhou, 510665, China. E-mail: lychris@sina.com*

12 h in the oven. The final $La_2O_2CO_3$:1%Tb^{3+} nanorods were collected after annealing the precursor products at 600 °C for 3 h in the muffle furnace. The carbon atom maybe come from carbon dioxide in air atmosphere.

Characterization

The X-ray diffraction (XRD) (Cu/Kα) patterns of samples were recorded on a PANAlytical X'Pert PRO X-ray polycrystal diffractometer. Transmission electron microscopy (TEM) images and scanning electron microscopy (SEM) images were obtained on a Thermo-Talos F200S and Hitach-SU8220, respectively. Dynamic light scattering spectrum of samples was performed on a Malvern Instruments-Zetasizer Nano ZS at 25 °C. The dispersant is ethanol. Room temperature photoluminescence (PL), PL excitation (PLE) spectra, afterglow spectrum and decay curves of samples were monitored on a high-resolution spectrofluorometer (UK, Edinburgh Instruments, FLS 980) equipped with a 500 W Xenon lamp as an excitation source, with a Hamamatsu R928P visible photomultiplier (250–850 nm). Thermoluminescence (ThL) spectrum of samples was measured on a FJ-427A TL meter (Beijing, China).

Results and discussions

Phase and crystal structure

The X-ray diffraction (XRD) patterns of samples are described in Fig. 1a. The XRD patterns of the host $La_2O_2CO_3$ are in good agreement with the hexagonal $La_2O_2CO_3$ phase (JCPDS No. 37-0804) and no impurity peak was detected. When small amount of Tb^{3+} doped in the host, the peak position remains unchanged but the main peak shape of the XRD patterns becomes wider. In $La_2O_2CO_3$, the La site (ionic radius: 0.127 nm, CN = 10) bonds to three category O atoms (three O sites: O_1, O_2, O_3), thus offering the applicable decahedron coordination LaO_{10} to attach the rare-earth emitter Tb^{3+} (ionic radius: 0.110 nm, CN = 9).[25] Tb^{3+} may replace La^{3+} lattice site in this architecture based on the ionic radius and LaO_{10} coordination configuration (Fig. 1b). It is possible that the peak of the doped sample is broadening owing to the substitution of the La^{3+} by the relatively size Tb^{3+}.

Morphology and texture

The size and morphology of $La_2O_2CO_3$:1%Tb^{3+} nanorods are investigated *via* scanning electron microscopy (SEM), transmission electron microscopy (TEM) and high-resolution TEM (HRTEM). As revealed in Fig. 2a, $La_2O_2CO_3$:1%Tb^{3+} sample is a kind of one-dimension rod-like nanomaterial with uniform dispersion. Additionally, the hydrodynamic size of $La_2O_2CO_3$:1%Tb^{3+} nanorods is measured *via* dynamic light scattering (DLS). It confirms that size distribution follows a normal distribution with average length 184.5 nm. The polydispersity index (PdI) value (0.248) shows that the sample is moderately polydisperse (Fig. 2b).[26] These results indicate that the precipitation method can successful compound well-dispersed PLNPs.

For further revealing the information on morphology and structural features of $La_2O_2CO_3$:1%Tb^{3+} nanorods, the TEM and HRTEM also be measured. Fig. 3a and b display the typical TEM images of $La_2O_2CO_3$:1%Tb^{3+} nanorods. It demonstrates that the diameter of nanorods is 15–20 nm and the length are 50–200 nm, which is in keeping with DLS result. Fig. 3c displays the HRTEM image of $La_2O_2CO_3$:1%Tb^{3+} nanorods. The lattice planes of nanorod are counted to be 2.0388 nm and 1.3299 nm, which belong to (110) and (211) crystallographic planes of $La_2O_2CO_3$, respectively. It indicates that $La_2O_2CO_3$:1%Tb^{3+} nanorod is polycrystalline while the different crystal

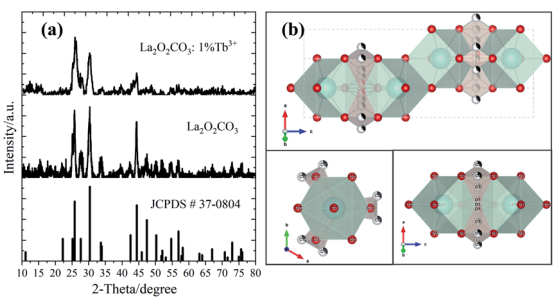

Fig. 1 XRD patterns (a) and crystal structure (b) of $La_2O_2CO_3$:1%Tb^{3+} sample.

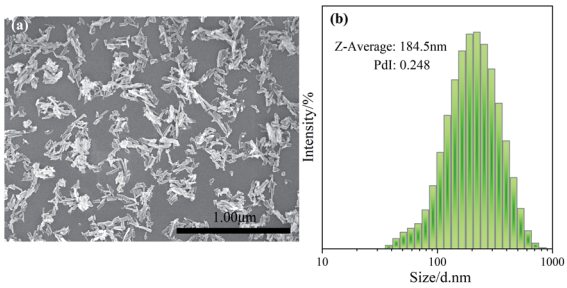

Fig. 2 SEM image (a) and dynamic light scattering (DLS) spectrum (b) of $La_2O_2CO_3$:1%Tb^{3+} sample.

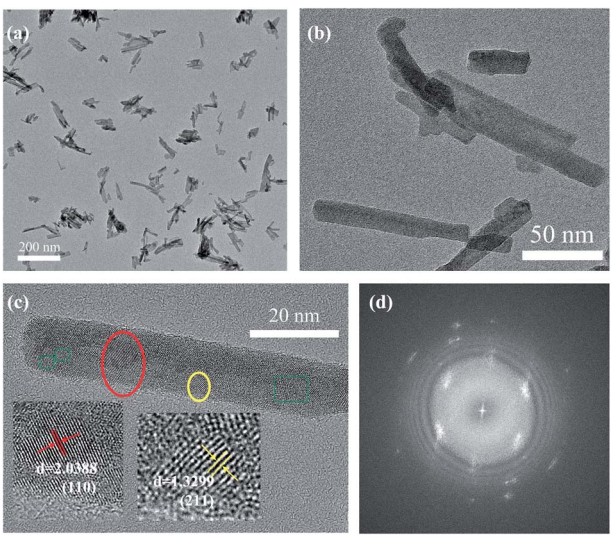

Fig. 3 TEM images (a and b), HRTEM image (c) and crystal diffraction spot image (d) of $La_2O_2CO_3$:1%Tb^{3+} sample.

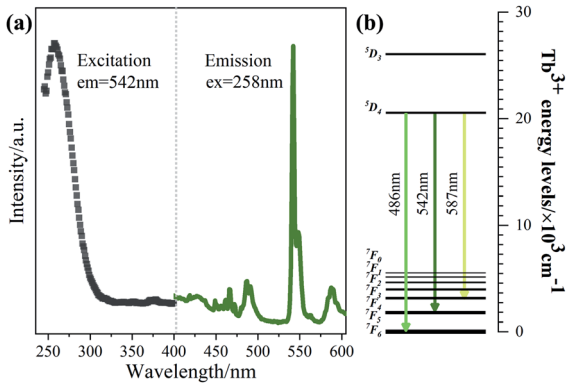

Fig. 4 The excitation and emission spectrum (a) and the energy levels image (b) of the $La_2O_2CO_3$:1%Tb^{3+} sample.

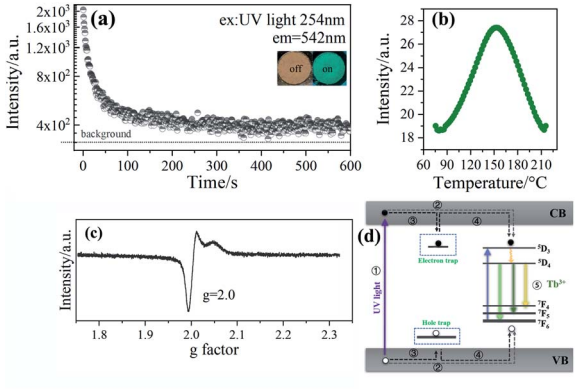

Fig. 5 The persistent luminescence spectrum (the duration time is 5 s between the turn-off of the excitation light and the beginning of the measurements, and measurement apparatus) (a), thermoluminescence spectrum (the scan rate is 2 K s^{-1}, and the duration time is 10 s between the turn-off of the excitation light and the beginning of the measurements for the TL measurements) (b), EPR spectrum (c) and the afterglow mechanism (d) of the $La_2O_2CO_3$:1%Tb^{3+} sample.

orientations can be found distinctly. The presence of indiscernible lattice fringes in $La_2O_2CO_3$ nanorod due to the formation of defects.[27] The crystal diffraction spot image of a single nanorod (Fig. 3d) insinuates that nanorod is polycrystalline, which matches greatly with the HRTEM results.

Photoluminescent properties

The excitation and emission spectra are used to illustrate the photoluminescent property of $La_2O_2CO_3$:1%Tb^{3+} nanorods (the doping content of 1% has been reported to be a suitable value for preparing Tb^{3+}-doped luminescent phosphors),[5,23,28,29] as shown in Fig. 4a. An evident excitation peak at 258 nm can be measured when monitoring at 542 nm emission at room temperature. It can be assigned to the spin allowed interconfigurational $4f^8$–$4f^75d^1$ transition of Tb^{3+}.[30–33] The emission spectrum of $La_2O_2CO_3$:1%Tb^{3+} covers a wide wavelength range between 400 nm and 600 nm. Peaks at 486 nm, 542 nm and 587 nm are observed, which can be ascribed by the 4f–4f transitions from $^5D_4$ to ^7F_J ($J = 6, 5, 4$). The blue emission peaks in 400–470 nm are attributed to the $^5D_3$ to ^7F_J ($J = 5, 4, 3$) transitions, respectively (Fig. 4b).[9,32,34–37] The bright green-light emitting belongs to the strongest transition $^5D_4$ to $^7F_5$ of largest probability for both forced electric dipole and magnetic dipole induced transitions.[13,36]

Persistent luminescence property

The afterglow decay curve of $La_2O_2CO_3$:1%Tb^{3+} sample is presented in Fig. 5a. It clearly reveals that the decay process includes a fast decay part and a slow decay process. A strong afterglow at 542 nm appear at the initial stage of fast decay while a long afterglow duration almost 600 s after ceasing the UV-light irradiation support the existing slow decay. The color of the sample is yellow-color possibly due to the existence of extra tetravalent terbium ions (Tb^{4+}).[38] Particularly, no feature fluorescence of Tb^{4+} are found in Fig. 4a, because it may play the role of ionic impurities. It is well-known that the generation of long persistent luminescence is primarily attributed to the capture of excited electrons *via* creating traps in the host lattice.[1] The ThL curve can provide vital information about the number, depth and density of traps,[39] which are advantageous to reveal the possible afterglow mechanism. Therefore, ThL curve of $La_2O_2CO_3$:1%Tb^{3+} sample is measured (Fig. 5b). Samples were excited at T_{exc} by 254 nm light for 20 min, the heating rate of 2 K s^{-1}. ThL spectrum consists a broad band locating at 424 K. The depths and densities of traps can be estimated by the following equations:[40] $E = T_m/500$ (where E is the thermo-active energy of trap depths (in eV) denoting the energy gap between the electron trap and the conduction band, and T_m is the ThL peak temperature in kelvin). The trap depth of $La_2O_2CO_3$:1%Tb^{3+} is 0.848 eV.

Electron spin resonance (ESR) is an effective and direct characterization to analysis varied behaviours of defects.[13,26] Fig. 5c exhibits the ESR test result of $La_2O_2CO_3$:1%Tb^{3+} sample. It can be seen an ESR signal at $g = 2.0$, which is close to free electrons generating from oxygen vacancies ($V_O^{\cdot\cdot}$).[26,41–43] $V_O^{\cdot\cdot}$ is a common electron-trap in oxide long afterglow phosphors.[44]

The terbium ions in the $La_2O_2CO_3$ host lattice would substitute the La^{3+}. Hence, when most of Tb^{3+} ions entered La^{3+} site, the neutral defect sites ($Tb_{La}^{\times}$) will be given as eqn (1):[36,44]

$$Tb^{3+} + La^{3+} \rightarrow Tb_{La}^{\times} \quad (1)$$

On the other hand, the Tb^{4+} impurities also have chance to substitute the La^{3+}, the unbalanced substitution occurred as eqn (2):[36,45]

$$2Tb^{4+} + 3La^{3+} \rightarrow 2Tb_{La}^{\cdot} + V_{La}'' \quad (2)$$

The Tb ions with a positive net charge ($Tb_{La}^{\cdot}$) acted as electron-traps. Meanwhile, a charge compensation is coming out owing the unequally charges possibly.[46] It means a simultaneous creation of a La^{3+} vacancy (V_{La}''), which acted as hole-traps.

Based on experimental results of afterglow properties, doping Tb^{3+} ions not only acted as an activator but also formed

point defects ($Tb_{La}^{\times}$). The Tb^{4+} impurities not only changed the sample's color, but also created electron-traps ($Tb_{La}^{\bullet}$) and hole-traps (V_{La}''). A possible diagrammatic drawing of $La_2O_2CO_3$:1% Tb^{3+} afterglow mechanism is shown in Fig. 5d. To explain, the Tb^{3+} energy levels are putted between the conduction band (CB) and valence band (VB). The band gap of $La_2O_2CO_3$ is 5.83 ev.[24] During ultraviolet (UV) light irradiation (①), most of the excited electrons and holes are transferred through the CB and VB to the luminescence centers of Tb^{3+} respectively (②), and then causing the characteristic emissions of Tb^{3+} (⑤). However, some of the excited electrons and holes will be captured by electron-traps ($V_O^{\bullet\bullet}$, $Tb_{La}^{\times}$, $Tb_{La}^{\bullet}$) from CB or hole-traps (V_{La}'') from VB through non-radiative transition respectively (③). Then, the stored electrons and holes can escape from the traps by the proper thermal activation, and the released energy be transferred to Tb^{3+} ions *via* the VB and CB (④). Then the afterglow of Tb^{3+} (⑤) is appearing.

Conclusions

In this paper, the $La_2O_2CO_3$:1%Tb^{3+} PLNPs have been synthesized *via* a facile precipitation method. The morphology and texture of $La_2O_2CO_3$:1%Tb^{3+} sample display uniform dispersion and rod-like shape. The strongest emission peak locates at 542 nm which attributes to $^5D_4$ to $^7F_5$ transition. The green afterglow at 542 nm can be detected almost 600 s after ceasing the UV-light irradiation. ThL measurement reveals that $La_2O_2CO_3$:1%Tb^{3+} sample possesses one shallow trap depth calculated to be 0.848 eV. The results show that the one-dimensional nanorods with green long afterglow can be successfully synthesized *via* a simple precipitation method.

Conflicts of interest

There are no conflicts to declare.

Acknowledgements

This work was financially supported by the National Natural Science Foundation of China (Grant No. 51602063), Guangdong Natural Science Foundation (Grant No. 2019A030310444), and Science and Technology Program of Guangzhou (201804010257). This work was also supported by Guangdong High-level personnel of special support program and Open Fund of the State Key Laboratory of Luminescent Materials and Devices (South China University of Technology).

References

1 Y. Li, M. Gecevicius and J. Qiu, *Chem. Soc. Rev.*, 2016, **45**, 2090–2136.
2 J. Wang, Q. Ma, X.-X. Hu, H. Liu, W. Zheng, X. Chen, Q. Yuan and W. Tan, *ACS Nano*, 2017, **11**, 8010–8017.
3 Z. Pan, Y.-Y. Lu and F. Liu, *Nat. Mater.*, 2012, **11**, 58–63.
4 Z. Yan, Z. R. xia, Z. Xia, R. X. guang, H. Z. dong and Z. J. hua, *Chin. J. Lumin.*, 2010, **31**, 489–492.
5 M. Li, X. Yu, T. Wang, J. Qiu and X. Xu, *Ceram. Int.*, 2015, **41**, 11523–11527.
6 Y. Teng, J. Zhou, S. N. Khisro, S. Zhou and J. Qiu, *Mater. Chem. Phys.*, 2014, **147**, 772–776.
7 H. Li, R. Pang, S. Zhang, L. Lv, J. Feng, L. Jiang, D. Li, C. Li and H. Zhang, *Dalton Trans.*, 2018, **47**, 9814–9823.
8 Y. Liang, F. Liu, Y. Chen, K. Sun and Z. Pan, *Dalton Trans.*, 2016, **45**, 1322–1326.
9 G. Ju, Y. Hu, L. Chen, Z. Yang, T. Wang, Y. Jin and S. Zhang, *Ceram. Int.*, 2015, **41**, 14998–15004.
10 C. C. Pedroso, J. M. Carvalho, L. C. Rodrigues, J. Holsa and H. F. Brito, *ACS Appl. Mater. Interfaces*, 2016, **8**, 19593–19604.
11 B.-g. Zhai and Y. M. Huang, *J. Mater. Sci.: Mater. Electron.*, 2017, **52**, 1813–1822.
12 M.-H. Lee and W.-S. Jung, *Bull. Korean Chem. Soc.*, 2013, **34**, 3609–3614.
13 B. Lei, B. Li, H. Zhang, L. Zhang, Y. Cong and W. Li, *J. Electrochem. Soc.*, 2007, **154**, H623–H630.
14 J. Trojan-Piegza, J. Niittykoski, J. Hölsä and E. Zych, *Chem. Mater.*, 2008, **20**, 2252–2261.
15 A. Escudero, A. I. Becerro, C. Carrillocarrion, N. O. Nunez, M. V. Zyuzin, M. Laguna, D. Gonzalezmancebo, M. Ocana and W. Parak, *Nanophotonics*, 2017, **6**, 881–921.
16 H.-X. Mai, Y.-W. Zhang, R. Si, Z.-G. Yan, L.-d. Sun, L.-P. You and C.-H. Yan, *J. Am. Chem. Soc.*, 2006, **128**, 6426–6436.
17 Y. Xia, *Nat. Mater.*, 2008, **7**, 758–760.
18 B. B. Srivastava, A. Kuang and Y. Mao, *Chem. Commun.*, 2015, **51**, 7372–7375.
19 E. Teston, S. Richard, T. Maldiney, N. Lievre, G. Y. Wang, L. Motte, C. Richard and Y. Lalatonne, *Chem.–Eur. J.*, 2015, **21**, 7350–7354.
20 Z. Li, Y. Zhang, X. Wu, L. Huang, D. Li, W. Fan and G. Han, *J. Am. Chem. Soc.*, 2015, **137**, 5304–5307.
21 Z. Zhou, W. Zheng, J. Kong, Y. Liu, P. Huang, S. Zhou, Z. Chen, J. Shi and X. Chen, *Nanoscale*, 2017, **9**, 6846–6853.
22 H. Liu, X. Hu, J. Wang, M. Liu, W. Wei and Q. Yuan, *Chin. Chem. Lett.*, 2018, **29**, 1641–1644.
23 G. Li, C. Peng, C. Zhang, Z. Xu, M. Shang, D. Yang, X. Kang, W. Wang, C. Li and Z. Cheng, *Inorg. Chem.*, 2010, **49**, 10522–10535.
24 X. Dou, Y. Li, T. Vaneckova, R. Kang, Y. Hu, H. Wen, X. Gao, S. Zhang, M. Vaculovicova and G. Han, *J. Lumin.*, 2019, **215**, 116635.
25 R. D. Shannon, *Acta Crystallogr., Sect. A: Cryst. Phys., Diffr., Theor. Gen. Crystallogr.*, 1976, **32**, 751–767.
26 S. Bhattacharjee, *J. Controlled Release*, 2016, **235**, 337–351.
27 F. Dong, X. Xiao, G. Jiang, Y. Zhang, W. Cui and J. Ma, *Phys. Chem. Chem. Phys.*, 2015, **17**, 16058–16066.
28 H. Luo, A. J. Bos and P. Dorenbos, *J. Phys. Chem. C*, 2017, **121**, 8760–8769.
29 L. C. Rodrigues, H. F. Brito, J. Hölsä, R. Stefani, M. C. Felinto, M. Lastusaari, T. Laamanen and L. A. Nunes, *J. Phys. Chem. C*, 2012, **116**, 11232–11240.
30 Y. Mayama, T. Masui, K. Koyabu and N. Imanaka, *J. Alloys Compd.*, 2008, **451**, 132–135.
31 T. Masui, K. Koyabu, S. Tamura and N. Imanaka, *J. Mater. Sci.: Mater. Electron.*, 2005, **40**, 4121–4123.

32 C. Liu, G. Che, Z. Xu and Q. Wang, *J. Alloys Compd.*, 2009, **474**, 250–253.
33 S. X. yuan, F. X. xuan, H. J. jie, L. Q. song, J. G. yuan, D. Yun, L. Y. shi and W. C. lei, *Chin. J. Lumin.*, 2020, **41**, 265–270.
34 J. Cao, X. Wang, X. Li, Y. Wei, L. Chen and H. Guo, *J. Lumin.*, 2016, **170**, 207–211.
35 J. Santos, E. Silva, N. Souza, Y. Alves, D. Sampaio, C. Kucera, L. Jacobsohn, J. Ballato and R. Silva, *Ceram. Int.*, 2019, **45**, 3797–3802.
36 X. Fu, S. Zheng, J. Shi, Y. Li and H. Zhang, *J. Lumin.*, 2017, **184**, 199–204.
37 L. Z. qiu, Z. J. su, L. X. ping, S. J. shi, C. L. hong, Z. H. yang and C. B. jiu, *Chin. J. Lumin.*, 2013, **34**, 30–34.
38 J. Kaszewski, B. S. Witkowski, Ł. Wachnicki, H. Przybylińska, B. Kozankiewicz, E. Mijowska and M. Godlewski, *J. Rare Earths*, 2016, **34**, 774–781.
39 X. Lin, R. Zhang, X. Tian, Y. Li, B. Du, J. Nie, Z. Li, L. Chen, J. Ren, J. Qiu and Y. Hu, *Adv. Opt. Mater.*, 2018, **6**, 1701161.
40 Y. Li, S. Zhou, Y. Li, K. Sharafudeen, Z. Ma, G. Dong, M. Peng and J. Qiu, *J. Mater. Chem. C*, 2014, **2**, 2657–2663.
41 K. A. Alim, V. A. Fonoberov, M. Shamsa and A. A. Balandin, *J. Appl. Phys.*, 2005, **97**, 124313.
42 A. B. Djurišić, W. C. Choy, V. A. L. Roy, Y. H. Leung, C. Y. Kwong, K. W. Cheah, T. Gundu Rao, W. K. Chan, H. Fei Lui and C. Surya, *Adv. Funct. Mater.*, 2004, **14**, 856–864.
43 S. Zhang, S.-H. Wei and A. Zunger, *Phys. Rev. B: Condens. Matter Mater. Phys.*, 2001, **63**, 075205.
44 Z. Long, J. Zhou, J. Qiu, Q. Wang, D. Zhou, X. Xu, X. Yu, H. Wu and Z. Li, *J. Rare Earths*, 2018, **36**, 675–679.
45 Y. Jin, Y. Hu, C. Li, X. Wang, G. Ju and Z. Mu, *J. Lumin.*, 2013, **138**, 83–88.
46 X. Zhou, G. Ju, T. Dai and Y. Hu, *Opt. Mater. Express*, 2019, **96**, 109322.